Coupling of Energy Into PCB Traces in a Reverberant Environment: Absorption Cross-section and Probability of Susceptibility

Arunkumar H. Venkateshaiah
Department of Electronic Engineering
University of York
York, UK
https://orcid.org/0000-0002-3505-1970

Haiyan Xie
Northwest Institute of NuclearTechnology
Shaanxi, China
xiehaiyan@nint.ac.cn

John F. Dawson
Department of Electronic Engineering
University of York
York, UK
john.dawson@york.ac.uk

Andrew C. Marvin
Department of Electronic Engineering
University of York
York, UK
andy.marvin@york.ac.uk

Linda Dawson
Department of Electronic Engineering
University of York
York, UK
l.dawson@york.ac.uk

Martin P. Robinson
Department of Electronic Engineering
University of York
York, UK
martin.robinson@york.ac.uk

***Abstract*—Predicting the probability of susceptibility to electromagnetic interference for a system would be of significant interest to the EMC community. In this paper, we consider the coupling of electromagnetic energy into printed circuit board (PCB) traces and how it relates to the power balance model of shielding effectiveness. We show results of some measurements of the absorption cross-section of a load on a PCB trace and compare them with previously published results.**

Keywords—Absorption cross-section, Electromagnetic Interference, Electromagnetic Shielding, Reverberation Chamber

I. Introduction

In previous work, we have considered the effect of contents on the shielding effectiveness (SE) of enclosures [1–4] and measured the average absorption cross-section (AACS) of printed circuit boards [2,5,6] so that their effect on SE can be determined. Recently we have considered how individual Printed circuit board (PCB) traces and their attached loads contribute to the absorption cross-section [1,7]. This is of interest as it may be useful in computing the AACS of circuit boards from knowledge of their layout, and also because it has the potential to allow the energy absorbed into their loads to be determined, and thus predict the likelihood of the energy absorbed causing a failure due to the susceptibility of a component.

In this paper, we present a methodology for the prediction of immunity of circuits in electrically large, reverberant enclosures, based on the power balance method [8,9]. In Section II, we summarise the essentials of the power balance method for determining SE. In Section III, we summarise possible techniques for predicting trace AACS. In Section IV, we describe the methodology for measuring the AACS of a PCB track, and in Section V, we compare the measured AACS of some simple PCB tracks with that predicted by analytic, semi-analytic and full-wave numerical solvers. In Section VI, we discuss possible future work to complete and validate the methodology and present our conclusions.

The research leading to these results has received funding from the European Union's Horizon 2020 research and innovation programme under the Marie Skłodowska-Curie grant agreement No 812.790 (MSCA-ETN PETER). This publication reflects only the author's view, exempting the European Union from any liability. Project website: http://etn-peter.eu/. The work of H Xie was supported by the China Scholarship Council (201803170037)

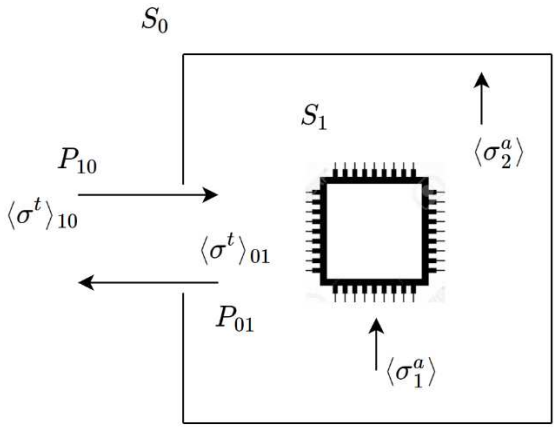

Fig. 1. Power flow in an enclosure.

II. Shielding Effectiveness and Power Balance Method

A. Shielding Effectiveness

There are many ways to define the SE of an enclosure, however, in this paper we define SE in terms of power densities. SE is the ratio of power density outside (S_0) to the power density inside an enclosure (S_1):

$$\mathrm{SE} = \frac{S_0}{S_1} \tag{1}$$

The power density is directly proportional to the square of the total electric field and is given by [8]:

$$S = \frac{{E_0}^2}{\eta_0} \tag{2}$$

where E_0 is the total electric field and η_0 is the intrinsic impedance of free space.

B. The Power Balance Method

Power balance analysis is a technique to estimate the electromagnetic power flow and energy inside an enclosure or set of coupled enclosures [7]. Fig. 1 shows the flow of power in an enclosure. The power flow through an aperture depends only on the power density on each side of it and its transmission cross-section:

$$P_{10} = S_0\langle\sigma^t\rangle \text{ and } P_{01} = S_1\langle\sigma^t\rangle \tag{3}$$

978-1-7281-5579-1/20/$31.00 ©2020 IEEE

where $\langle\sigma^t\rangle = \langle\sigma_{10}^t\rangle = \langle\sigma_{01}^t\rangle$ in the reverberant case [10], and is the transmission cross-section averaged over all angles of incidence and polarisations. The power absorbed by an object, such as the contents of the enclosure in Fig. 1, depends only on its AACS, $\langle\sigma^a\rangle$, and the power density incident on it:

$$P_a = S_1\langle\sigma^a\rangle \tag{4}$$

From that, we can write, in the steady-state, the power balance equation for a scenario such as Fig. 1:

$$P_{10} = P_{01} + P_a \tag{5}$$

The power entering the enclosure must be the sum of the power leaving it and the power absorbed inside it.

$$S_0\langle\sigma^t\rangle = S_1\langle\sigma^t\rangle + S_1\sum\langle\sigma^a\rangle \tag{6}$$

where $\sum\langle\sigma^a\rangle$ is the sum of all the AACSs of the enclosure contents, and walls. The SE of the enclosure can then be written purely in terms of the transmission and absorption cross-sections:

$$\mathrm{SE} = \frac{S_0}{S_1} = \frac{\langle\sigma^t\rangle + \sum\langle\sigma^a\rangle}{\langle\sigma^t\rangle} \tag{7}$$

III. Coupling to PCB Traces and IC Packages

Knowledge of the enclosure SE allows us to predict the internal fields, given the external fields. If we know the AACS of an individual track ($\langle\sigma_t^a\rangle$), we can then predict the energy absorbed into the terminals (P_t) of components attached to the track:

$$P_t = S_1\langle\sigma_t^a\rangle \tag{8}$$

The coupling of electromagnetic waves to transmission lines has been widely studied [11–13] in the case of a single plane wave and also recently in the case of a reverberant field [14–16]. In [7] we built on those ideas comparing a number of methods to compute the energy absorbed by PCB load tracks and their contribution to the PCB AACS. We will briefly review the methods described in [7] before comparing them with new measured data.

A. Numerical Monte Carlo Method

Using the analytic solution for a single plane wave [12] we emulated a reverberant environment by computing the power dissipated in the transmission line loads for a number of randomly chosen plane-waves, applied simultaneously, and averaged over a number of sets of plane–waves as described in detail in [7]. This is much faster than using a full-wave solver, but assumes an idealized geometry with an infinite ground plane.

B. Gauss-Legendre Quadrature combined with full-wave solver

Using a full-wave solver [17] we illuminated the track on a finite PCB with a number of plane waves chosen based on the Gauss-Legendre Quadrature method [1,18] to achieve optimum results with the minimum number of simulations. We found 64 individual plane wave simulations to be sufficient, but this requires a substantial amount of time to compute. The PCB model was of the same dimensions as used in the measurements in the next section.

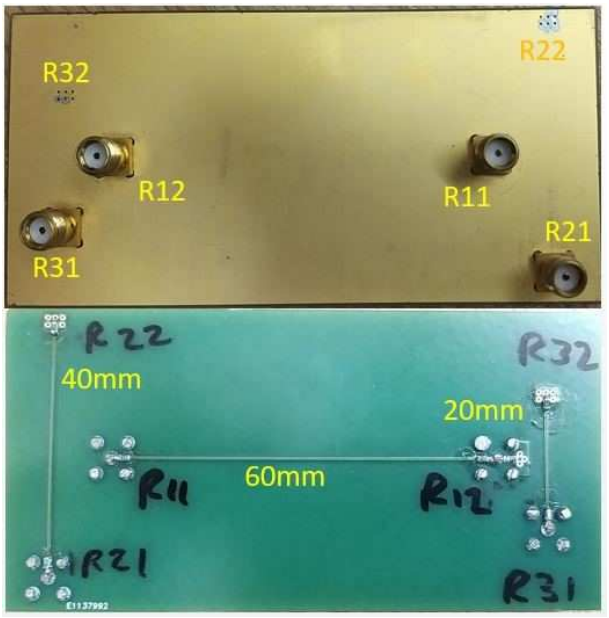

Fig. 2. PCB front and back.

IV. Experimental Method

A. Measurement of a lossy Microstrip TL on a PCB

A PCB with lossy microstrip transmission line (TL) traces as shown in Fig. 2 is used for the measurements. The dimensions of the PCB are 100 mm×50 mm and its substrate (FR-4) height is 1.55 mm. There are three traces on the PCB with different lengths (60 mm, 40 mm, and 20 mm) which are placed orthogonal to each other to minimize the coupling effect between them. Each trace has a width of 0.48 mm and a thickness of 18 µm. To measure the coupled signal there are four SMA connectors, one at each end of the long track, and one at one end of each of the shorter tracks, as shown in Fig. 2. To match the impedance of the measurement system ($Z_{\mathrm{VNA}} = 50\ \Omega$) to the characteristic impedance (115 Ω) of the traces an additional series resistance of 65 Ω is added near each SMA connector ($R_s = \mathrm{R11} = \mathrm{R12} = \mathrm{R21} = \mathrm{R31} = 65\ \Omega$). The ends of the 40 mm and 20 mm tracks without SMA connector have load resistances of $Z_L = R32 = R22 = 115\ \Omega$ to provide a matched termination.

B. Experimental Setup

Fig. 3. Experimental setup inside the reverberation chamber showing Antenna 1 behind stirrer with PCB and Antenna 2 on polystyrene block.

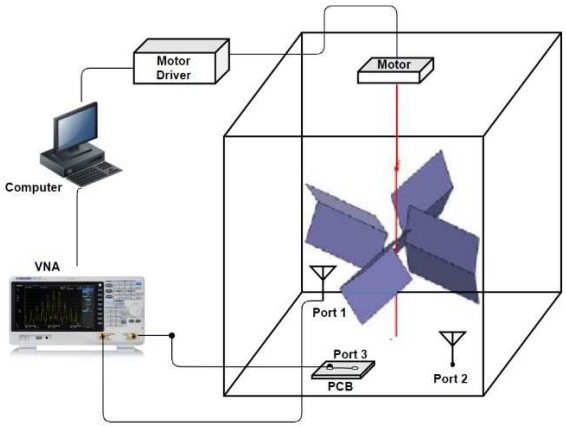

Fig. 4. Experiment Setup with trace connected

Fig. 3 shows a photograph and Fig. 4 shows a diagram of the experimental setup in the reverberation chamber. The dimensions of the reverberation chamber are 4.7 m × 3.0 m × 2.37 m. All the experiments are conducted using 100 stirrer positions, that is for every 3.6 degrees of stirrer rotation, frequency is swept from 500 MHz to 10 GHz and S-parameters between two VNA ports are measured with a frequency step of 1 MHz.

First, a calibration measurement is performed where both antennas in Fig. 4 are connected to port 1 and 2 of a vector network analyzer (VNA) and, the PCB is kept inside the reverberation chamber with 50 Ω loads attached to all four SMA connectors. The calibration described in Section IV C below.

Now, one of the PCB traces is connected to port 2 of the VNA as shown in and the unused antenna is terminated with a 50 Ω load. The power absorbed into a load on the trace can be computed as described in Section IV D.

C. Chamber Energy Density and Received Power

Fig. 5 shows the power flow interaction between two antennas coupled through a reverberation chamber, typical backscattered and reciprocal rays for antenna 1 and typical ray propagating from antenna 1 to 2, along with energy absorbed into the contents are shown. By measuring the S-parameters between two antennas in the chamber, with the PCB inside, and terminated with 50Ω loads, the chamber energy density for an arbitrary forward power can be determined.

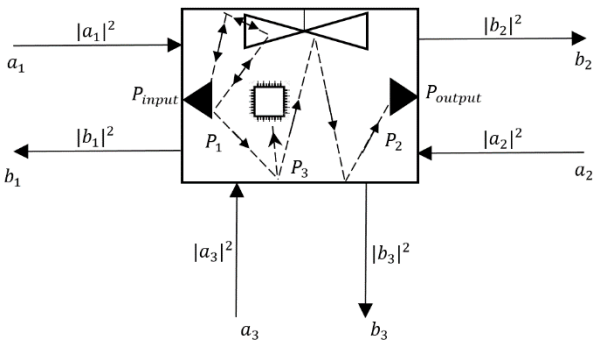

Fig. 5. Power flow in the reverberation chamber.

As used in S-parameter notation the forward power flow towards the left-hand antenna 1 is $|a_1|^2$, and the reverse power is $|b_1|^2$. Similarly at the right-hand antenna 2, the forward (towards antenna) and reverse (from antenna) powers are $|a_2|^2$ and $|b_2|^2$ respectively. The average power entering the chamber over a number of stirrer positions is:

$$\langle P_1 \rangle = (\langle |a_1|^2 \rangle - |\langle b_1 \rangle|^2)\eta_1$$
$$= \langle |a_1|^2 \rangle (1 - |\langle S_{11} \rangle|^2)\eta_1 \quad (9)$$

where η_1 is the radiation efficiency of the antenna and $\langle S_{11} \rangle$ is the mean of the measured antenna reflection coefficient which is the same as the antenna free-space reflection coefficient [19]. Similarly, for the receiving antenna, the power to its load is reduced by its radiation efficiency (η_2) and any mismatch to its load, which is in magnitude equal to the antenna reflection coefficient (S_{22}) so the average power $\langle |b_2|^2 \rangle$ is the power from antenna 2 reduced by the mismatch and antenna efficiency:

$$\langle |b_2|^2 \rangle = \langle P_2 \rangle (1 - |\langle S_{22} \rangle|^2)\eta_2 \quad (10)$$

Now from the received power, averaged over a number of stirrer positions, $\langle P_2 \rangle$, we can deduce the chamber total field:

$$E_0^2 = \frac{8\pi\eta_0\langle P_2 \rangle}{\lambda^2} \quad (11)$$

where η_0 is the characteristic impedance of free space and λ is the free-space wavelength. Similarly, the power density in the chamber is:

$$S_0 = \frac{E_0^2}{\eta_0} = \frac{8\pi\langle P_2 \rangle}{\lambda^2} \quad (12)$$

From equation (9) and (10), we can write the P_2 in terms of the S-parameters and P_1 as shown below,

$$\langle P_2 \rangle = \frac{|S_{21}|^2}{(1-|\langle S_{11} \rangle|^2)\eta_1(1-|\langle S_{22} \rangle|^2)\eta_2} \langle P_1 \rangle$$
$$= G\langle P_1 \rangle \quad (13)$$

as $b_2/a_1 = S_{21}$ by definition, and G is the mean net transfer function of the chamber [20].

Since we require only the scattered component, we can remove any direct component ($|\langle S_{21} \rangle|$) from the computation by subtracting it from S_{21} before computing the average magnitude.

$$\langle P_2 \rangle = \frac{\langle |S_{21} - \langle S_{21} \rangle|^2 \rangle}{(1-|S_{11}|^2)(1-|S_{22}|^2)\eta_1\eta_2} \langle P_1 \rangle$$
$$= G'\langle P_1 \rangle \quad (14)$$

where G' is a modified mean net transfer function. The energy density (12) in the chamber can be written as:

$$S_0 = \frac{8\pi}{\lambda^2} G'\langle P_1 \rangle$$
$$= K\langle P_1 \rangle \quad (15)$$

We can consider K as a calibration factor for this specific arrangement.

D. Computation of Track AACS and Absorbed Power

If the coupling to the load on the end of the PCB track is measured we can now determine its AACS. As the load comprises a 65 Ω resistance in series with the track connector and the 50 Ω resistance of the measurement instrument as shown in Fig. 6 for the long track and Fig. 7 for the short tracks we must predict the overall power from the measured power.

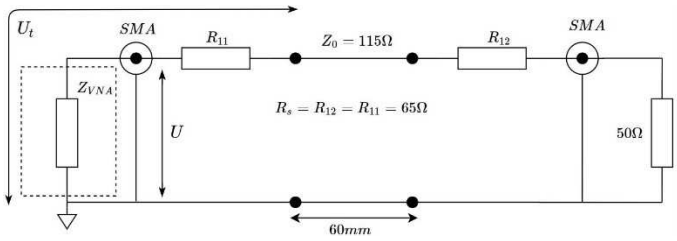

Fig. 6. Schematic diagram when one end of the 60 mm trace is connected to VNA.

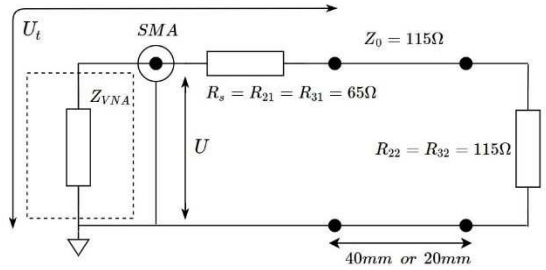

Fig. 7. Schematic diagram when one end of 40 mm or 20 mm trace is connected to VNA.

The power absorbed at the end of the trace P_a can be written in terms of power, P_3, measured by the measurement instrument.

$$P_a = P_3 \frac{(Z_{\text{VNA}}+R_S)}{Z_{\text{VNA}}} = P_1|S_{31} - \langle S_{31}\rangle|^2 \frac{(Z_{\text{VNA}}+R_S)}{Z_{\text{VNA}}} \quad (16)$$

where $Z_{VNA} = 50\ \Omega$ is the input impedance of VNA and S_{31} is the measured coupling between the antenna and track output connector.

Using the calibration factor determined in the previous section, the track AACS can therefore be written as:

$$\langle \sigma_t^a \rangle = \frac{\langle P_a \rangle}{S_0} = P_1 \langle |S_{31} - \langle S_{31}\rangle|^2 \rangle \frac{(Z_{VNA}+R_S)}{Z_{\text{VNA}}} \cdot \frac{1}{K\langle P_1 \rangle}$$
$$= \frac{\langle |S_{31} - \langle S_{31}\rangle|^2 \rangle}{K} \cdot \frac{(Z_{VNA}+R_S)}{Z_{\text{VNA}}} \quad (17)$$

V. Results

Here we compare the measured power and AACS with results computed using the methods described in Section III and [7].

A. Power Absorbed Into the Trace Loads

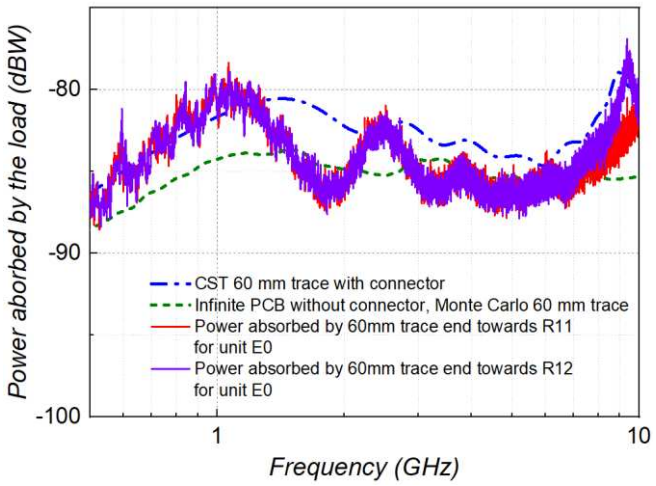

Fig. 8. Power absorbed by 60 mm trace matched loads for 1 V/m total field

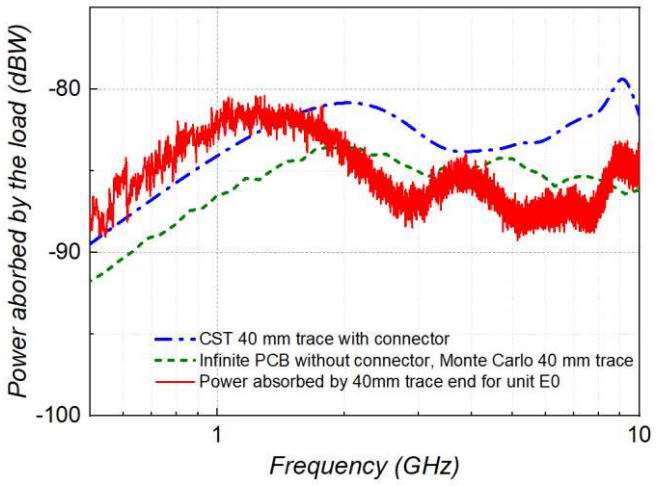

Fig. 9. Power absorbed by 40 mm trace matched loads for 1 V/m total field

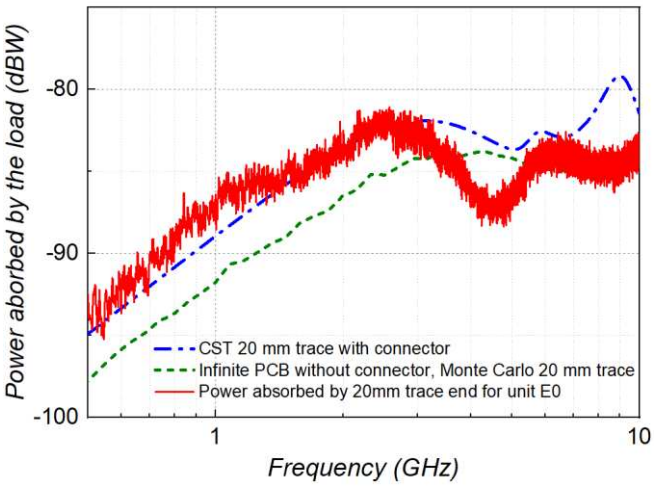

Fig. 10. Power absorbed by 20 mm trace matched loads for 1 V/m total field

Fig. 8 shows the measured power in the loads at each end of the 60 mm track, compared with that predicted using the methods described in [7]. As predicted in [7] the power absorbed increases with frequency up to just above 1 GHz when it exhibits some periodic oscillations which depend on the trace length but the overall trend levels out. The measurements are comparable to the full-wave solver [17] solution.

The full-wave solver and measured data predicts a slightly larger power than the Monte-Carlo solution. This is partly because the semi-analytic nature of the Monte-Carlo solution assumes that the trace is placed on an infinite ground-plane, whereas in the measured and simulated cases the ground-plane is finite (See [7] Fig. 5).

The measured power in the loads of the shorter tracks are shown in Fig. 9 and Fig. 10. It can be seen that as the trace length gets shorter, the frequency at which the power trend levels out increases but, all track lengths exhibit a comparable maximum power (See also [7] Fig. 7).

B. AACS of Tracks

The AACS of the load on each track is computed from the absorbed power for a given incident field:

$$\langle \sigma_t^a \rangle = \frac{\langle P_a \rangle}{S_0} = \langle P_a \rangle \frac{\eta_0}{E_0^2} \quad (18)$$

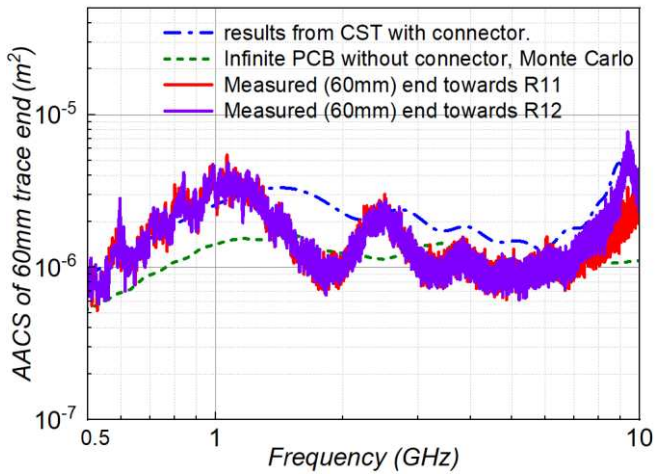

Fig. 11. AACS for 60 mm track with matched loads

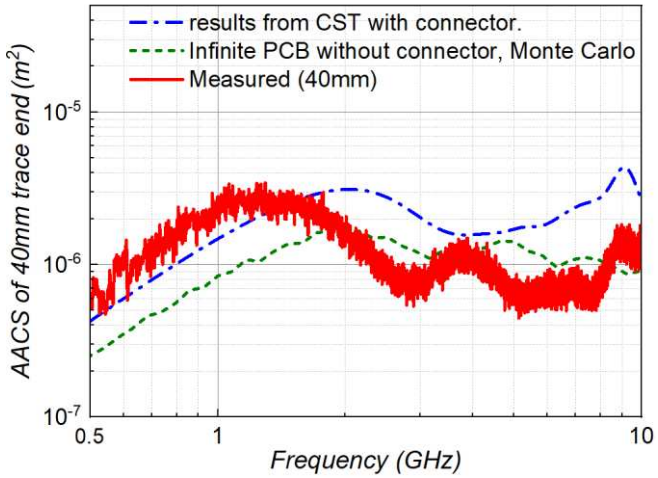

Fig. 12. AACS for 40 mm long track with matched loads

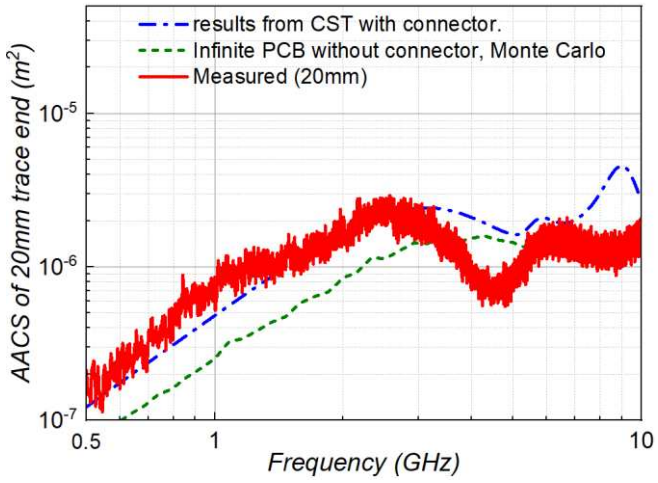

Fig. 13. AACS for 20 mm long track with matched loads

Fig. 11 to 13 show the AACS computed from the absorbed power results in Fig. 8 to 10.

VI. Conclusions and Further Work

We have presented an application of the power balance technique that might be used to predict the power absorbed into a component connected to a PCB trace. This along with IC immunity measurements such as described in standards such as [21] opens the possibility of predicting the probability of susceptibility of a circuit in a larger system.

The measurements described in this paper validate the predictions in [7]. Further work is required to predict the shadowing effect of nearby traces and components, to consider the effects of any energy coupled through the package itself and to develop and test methodologies for the assessment of the probability of susceptibility.

Acknowledgment

This project was undertaken on the Viking Cluster, which is a high performance compute facility provided by the University of York. We are grateful for computational support from the University of York High Performance Computing service, Viking and the Research Computing team

References

[1] I.D. Flintoft, S.J. Bale, A.C. Marvin, M. Ye, J.F. Dawson, M.Z. Changyong Wan, S.L. Parker, and M.P. Robinson, "Representative Contents Design for Shielding Enclosure Qualification from 2 to 20 GHz," *Electromagnetic Compatibility, IEEE Transactions on*, vol. 60, Feb. 2018, pp. 173–181.

[2] I.D. Flintoft, S.L. Parker, S.J. Bale, A.C. Marvin, J.F. Dawson, and M.P. Robinson, "Measured Average Absorption Cross-Sections of Printed Circuit Boards from 2 to 20 GHz," *Electromagnetic Compatibility, IEEE Transactions on*, vol. 58, Apr. 2016, pp. 553–560.

[3] A.C. Marvin, J.F. Dawson, S. Ward, L. Dawson, J. Clegg, and A. Weissenfeld, "A Proposed New Definition and Measurement of the Shielding Effect of Equipment Enclosures," *IEEE Transactions on Electromagnetic Compatibility*, vol. 46, 2004, pp. 459–468.

[4] D.W.P. Thomas, A. Denton, T. Konefal, T.M. Benson, C. Christopoulos, J.F. Dawson, A.C. Marvin, and J. Porter, "Characterisation of the Shielding Effectiveness of Loaded Equipment Enclosures," *Electromagnetic Compatibility, 1999. EMC York 99. International Conference and Exhibition on (Conf. Publ. No. 464)*, 1999, pp. 89–94.

[5] S.L. Parker, I.D. Flintoft, A.C. Marvin, J.F. Dawson, S.J. Bale, M.P. Robinson, M. Ye, C. Wan, and M. Zhang, "Predicting Shielding Effectiveness of Populated Enclosures Using Absorption Cross Section of PCBs," *2016 International Symposium on Electromagnetic Compatibility - EMC EUROPE*, 2016, pp. 324–328.

[6] S. Parker, I. Flintoft, A. Marvin, J. Dawson, S. Bale, M. Robinson, M. Ye, C. Wan, and M. Zhang, "Changes in a Printed Circuit Board's Absorption Cross Section Due to Proximity to Walls in a Reverberant Environment," *Electromagnetic Compatibility (EMC), 2016 IEEE International Symposium on*, Ottawa, Canada: 2016, pp. 818–823.

[7] H. Xie, J.F. Dawson, A.C. Marvin, and M.P. Robinson, "Numerical and Analytical Analysis of Stochastic Electromagnetic Fields Coupling to a Printed Circuit Board Trace," *Electromagnetic Compatibility, IEEE Transactions on*, 2019.

[8] D.A. Hill, M.T. Ma, A.R. Ondrejka, B.F. Riddle, and M.L. Crawford, "Aperture Excitation of Electrically Large, Lossy Cavities," *Electromagnetic Compatibility, IEEE Transactions on*, vol. 36, 1994, pp. 169–178.

[9] I. Junqua, J.-P. Parmantier, and F. Issac, "A Network Formulation of the Power Balance Method for High-Frequency Coupling," *Electromagnetics*, vol. 25, 2005, pp. 603–622.

[10] J.F. Dawson, A.C. Marvin, M. Robinson, and I.D. Flintoft, "On the Meaning of Enclosure Shielding Effectiveness," *2018 International Symposium on Electromagnetic Compatibility - EMC EUROPE*, Amsterdam: 2018, pp. 746–751.

[11] Y. Kami and R. Sato, "Circuit-Concept Approach to Externally Excited Transmission Lines," *IEEE Transactions on Electromagnetic Compatibility*, vol. EMC-27, Nov. 1985, pp. 177–183.

[12] M. Leone and H.L. Singer, "On the Coupling of an External Electromagnetic Field to a Printed Circuit Board Trace," *IEEE Transactions on Electromagnetic Compatibility*, vol. 41, Nov. 1999, pp. 418–424.

[13] C.R. Paul, “A Brief History of Work in Transmission Lines for EMC Applications,” *IEEE Transactions on Electromagnetic Compatibility*, vol. 49, May. 2007, pp. 237–252.

[14] M. Magdowski, G. Henning, and R. Vick, “Measurement of the Stochastic Electromagnetic Field Coupling to an Unshielded Twisted Pair Cable With a Matched Termination,” *ESA EMC Aerospace Workshop*, 2016.

[15] M. Magdowski, J. Kasper, R. Vick, I. Zalaliev, A. Ferenets, and others, “Electromagnetic Field Coupling to Transmission Line Networks of Double-Wire Lines in a Reverberation Chamber,” *2018 International Symposium on Electromagnetic Compatibility (EMC EUROPE)*, 2018.

[16] M. Mehri, N. Masoumi, and J. Rashed-Mohassel, “Trace Orientation Function for Statistical Prediction of PCB Radiated Susceptibility and Emission,” *Electromagnetic Compatibility, IEEE Transactions on*, vol. 57, Oct. 2015, pp. 1168–1178.

[17] “CST Studio Suite. 2019.,” [Online]. Available: www.3ds.com/products-services/simulia/products/cst-studio-suite: Dassault Systemes, .

[18] K. Atkinson, “Numerical Integration on the Sphere,” *J. Aust. Math. Soc. B*, vol. vol. 23, 1982, pp. 332–347.

[19] P.-S. Kildal, C. Carlsson, and J. Yang, “Measurement of Free-Space Impedances of Small Antennas In Reverberation Chambers,” *Microwave and Optical Technology Letters*, vol. 32, 2002, pp. 112–115.

[20] U. Carlberg, P.-S. Kildal, A. Wolfgang, O. Sotoudeh, and C. Orlenius, “Calculated and Measured Absorption Cross Sections of Lossy Objects in Reverberation Chamber,” *IEEE Transactions on Electromagnetic Compatibility*, vol. 46, May. 2004, pp. 146–154.

[21] *IEC 62132-4:2006, Integrated circuits - Measurement of electromagnetic immunity 150 kHz to 1 GHz - Part 4: Direct RF power injection method*, 2006.